

# A COMPARATIVE ANALYSIS OF THE AERODYNAMIC PERFORMANCE OF SUPERSONIC MISSILES WITH CONICAL AND OGIVE NOSE SHAPES

Mahdi GOUCEM <sup>1</sup>, Raouf KHIRI <sup>2</sup>

<sup>1</sup>Department of Mechanical Engineering, Usto University, BP. 1505 El M'Naouer, 31000 Oran, Algeria


<sup>2</sup>Department of Mechanical and Industrial Engineering, NOVA School of Science and Technology, 2829-516 Lisboa, Portugal

## Article History:

- received 28 April 2024
- accepted 27 August 2024

**Abstract.** This paper presents a numerical study conducted to analyze the aerodynamic performance of supersonic missiles consisting of a cylindrical body and four flat-plate rear fins arranged uniformly, equipped with conical and ogive heads. Computational Fluid Dynamics (CFD) simulations were performed using the ANSYS Fluent 17.1 solver, along with the Gambit grid generation software. The objective was to compare the aerodynamic characteristics of these two head designs in terms of drag, lift, and stability at supersonic speeds. Various flow parameters, including Mach number and angle of attack, were investigated to comprehensively assess the performance of the missile configurations. The results indicate clear differences in the aerodynamic behavior of conical and ogive heads. Specifically, there was a 2–11 percent increase in the lift coefficient of the conical heads compared to the ogive heads, and an increase in the drag coefficient of both conical and ogive heads.

**Keywords:** supersonic missile, conical and ogive heads, CFD simulations, aerodynamic coefficients, Mach number, angle of attack.

 Corresponding author. E-mail: [mahdi.goucem@univ-usto.dz](mailto:mahdi.goucem@univ-usto.dz)

## 1. Introduction

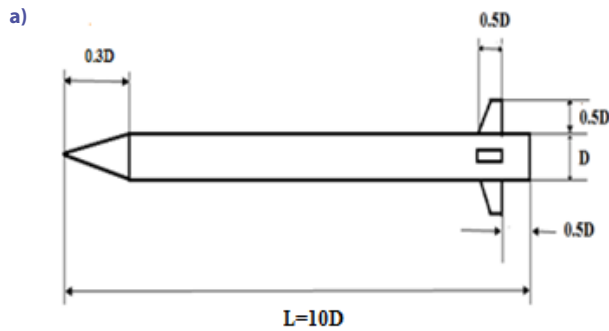
Missile aerodynamics stands as a cornerstone in the development and efficacy of a wide array of missile systems, spanning from tactical applications to intercontinental ballistic missiles. The intricate interplay between airflow dynamics, vehicle geometries, propulsion mechanisms, and control surfaces necessitates a multidisciplinary approach drawing from fluid dynamics, thermodynamics, and control theory. Divakaran et al. (2020) conducted a comprehensive study on the V-2 missile, utilizing ANSYS modeler to simulate the flow around the missile body and evaluate the effects of varying angles of attack and Mach numbers. The study demonstrated that the missile's aerodynamic efficiency was maintained at high velocities, even at significant angles of attack, due to the stable pressure coefficient and the strategic placement of the center of gravity and the center of pressure. Karpenko et al. (2023) studied hydraulic processes in transport machine hydraulic drives, focusing on fluid flow after installing angular fittings in pipelines. Using 3D numerical simulations based on Reynolds-averaged Navier–Stokes equations, they examined flow rates up to 100 l/min. Their mesh independence study ensured accuracy, and they analyzed pressure drops, turbulence models, flow coefficients, and energy losses at 45°

and 90° fittings. Comparing their results with the standard equivalent length fitting method, they found it unsuitable for angular fittings, suggesting the need for further investigation of each fitting type. Goucem and Khiri (2023) present a comprehensive analysis of the aerodynamic features of an air-to-air rocket, employing a cylindrical body with a tapered nose, four flat plates at the front, and four uniformly arranged flat-plate rear fins. Their study thoroughly investigated the impact of canard deflection angles on aerodynamic forces using computational fluid dynamics techniques, providing valuable insights into enhancing the efficiency of supersonic rockets. Doig (2014) reviewed the aerodynamics of bodies traveling close to the ground in transonic and supersonic regimes, focusing on applications such as wings, aircraft, projectiles, and rocket sleds. Their work highlighted the complexities of shock-related ground effects and the challenges in conducting accurate ground effect tests. They emphasized the need for high-fidelity experimental data and advanced numerical methods like LES to better understand shock/ground interactions, particularly for high-speed ground transportation and reusable spacecraft. Almawla et al. (2022) conducted a study that explores Computational Fluid Dynamics (CFD), a numerical method for approximating solutions to fluid motion equations, unfolded in four key stages. Firstly,

fluid flow equations are formulated as partial differential equations. Then, they undergo discretization to obtain numerical equivalents, followed by the subdivision of the fluid domain into small elements or cells. Finally, the problem equation is solved, considering initial and boundary conditions, employing solvers such as the Finite Volume Method (FVM), Finite Element Method (FEM), or Finite Difference Method (FDM). Karpenko and Bogdevičius (2020) investigated hydrodynamic processes in hydraulic drives of vehicles and machinery. They analyzed turbulent fluid flow through a “pipeline-fittings” system using numerical solutions of the Navier–Stokes equations. Their research focused on flow rates between 20 and 60 l/min, 1/2” pipeline diameters, and DKOL standard fittings. They modeled fluid pulsations and turbulence and experimentally studied hydraulic losses with one, two, and three fittings. Şumnu et al. (2020) provide a comprehensive tool for CFD fundamentals, governing equations, and turbulence models, demonstrating the effects of shape optimization on missile performance at supersonic speeds. The N1G missile model’s shape variation, aimed at reducing aerodynamic drag and increasing lift, was investigated using SST k- $\omega$ , realizable k- $\epsilon$ , and Spalart-Allmaras turbulence models. Optimization of missile geometry employed a Multi-objective Genetic Algorithm (MOGA) to improve lift-to-drag coefficient ratio by 11–17 percent at supersonic Mach numbers. Khanolkar et al. (2018) aimed to comprehend the aerodynamic traits of a medium-range air-to-air missile. Aerodynamic coefficients were derived via theoretical methods, wind tunnel tests, and computational fluid dynamics, with full-scale rocket models tested in the wind tunnel. The error-free data were analyzed using CFD to discern aerodynamic variations at different angles of attack, generating various graphs. Additionally, theoretical methods were used to gauge axial and normal forces on the missile at diverse angles of attack, followed by a comparative analysis between experimental, CFD, and theoretical data, revealing and studying nonlinearities to infer the missile’s performance. Yi et al. (2021) investigated the dynamic characteristics of missiles with variable swept-back angles using CFD simulations. Their study revealed that adjusting the sweep angle of missile wings significantly impacts lift and drag forces, enhancing aerodynamic performance at different flight speeds. They concluded that increasing the sweep angle improves the lift-drag ratio for missiles traveling at Mach numbers between 1 and 3, making it suitable for high-speed precision attacks. However, at Mach numbers greater than 3, a sweep angle of 60° was optimal. Yi et al. (2021) highlighted the advantages of deforming-wing technology for adapting to various flight conditions, thereby saving fuel and increasing attack range. Li et al. (2020) investigated how altering the sweep of variable-sweep folding wing missiles enhances their lift-drag ratio, enabling adaptation to subsonic, transonic, and supersonic flights. Designing various 3D models, they conducted aerodynamic analysis via CFD, adhering to Basic Aerodynamics, Missile General Design

Principles, and Flight Dynamics of Missiles principles. Their simulation analysis identifies optimal wing sweeps for diverse flight conditions. Sahbon et al. (2022) conducted CFD campaigns on two sounding rockets, FoK and Twardowsky, developed by the Students’ Space Association of Warsaw University of Technology. They created a mathematical model of aerodynamic loads and analyzed aerodynamic coefficients for various Mach numbers and incidence angles. The results showed good agreement, although improvements were suggested, such as considering varying aerodynamic roll angles and enhancing models of lift and pitching/yawing moments. The study emphasized the importance of detailed simulations and improved computational methods for accurate aerodynamic analysis. Ruchała et al. (2019) report wind tunnel tests of the Institute of Aviation’s Experimental Rocket Platform (ERP), designed for nearly 150 seconds of microgravity with an apogee of about 100 km. The ERP model was tested in the T-3 wind tunnel, assessing aerodynamic loads at angles of up to 10° of attack and various longitudinal axis rotations. Three configurations were tested: without fins and boosters, with fins only, and with both fins and boosters. Particle Image Velocimetry (PIV) measured velocity fields, revealing that boosters significantly increase aerodynamic drag and providing insights into rocket performance and stability. Bin-Dahalan et al. (2017) explore the aerodynamic traits of a curved fin rocket, employing semi-empirical methods and numerical simulations. The study integrates USAF DATCOM as a reference for the semi-empirical approach, while ANSYS Fluent is used for numerical simulations. Investigated across various Mach numbers ranging from 0.15 to 2.0 for subsonic and supersonic speeds, respectively, and angles of attack from 0° to 25°, the study compares results with wind tunnel tests, USAF DATCOM, and previous research, revealing consistent trends in rocket aerodynamics across methods. Chen et al. (2017) investigated the rolling characteristics of a canard-controlled rocket with a free-spinning tail using 3D Navier–Stokes equations and sliding mesh technology. They validated their simulation method through comparison with experimental results and proposed a convergence criterion, analyzing roll moment coefficients and induced rotation speed. The study demonstrated how the free-spinning tail eliminates roll coupling, providing insights for rocket design and simulation. Marciniak et al. (2023) discuss evaluating a Recovery System for the ILR-33 AMBER suborbital rocket, emphasizing a successful subsonic drop test campaign that qualified the system for the first AMBER rocket version. They present analytical and numerical methods for recovery development, underscoring the pivotal role of drop tests in providing essential data for redesign and confirming the feasibility of a three-stage parachute recovery concept. Julian et al. (2023) conducted a numerical study on R-HAN 122 rocket aerodynamics, focusing on nose shape modification using computational methods. Their analysis, employing RANS equations and a k- $\epsilon$  turbulence model, features a two-dimensional approach with

a structured mesh of  $2 \times 10^5$  elements. The study reveals that cone and hemisphere shapes enhance the lift coefficient (Cl) at  $4^\circ < \text{AoA} < 10^\circ$  but increase the drag coefficient (Cd) for R-HAN 122, with varying pressure distributions along different nose shapes. Ghoreyshi et al. (2022) investigated missile configurations with upstream strakes and cruciform all-movable tail fins, using CFD to simulate angles of attack from  $0^\circ$  to  $15^\circ$  and Mach numbers of 1.17, 2.49, and 4.39. They compared force and moment coefficients across different configurations, showing good agreement with wind tunnel data and highlighting CFD as a valuable complement to wind tunnel experiments, especially under uncertain conditions. Şumnu and Guzelbey (2023) investigated missile aerodynamics at subsonic and transonic speeds, examining different wing configurations. The Tapered Leading Edge wing showed superior lift-to-drag ratio compared to the Tapered Trailing Edge and Double Tapered configurations. Performance improved by about 5% at 0.9 Mach compared to 0.7 Mach across all configurations. The study used detailed 3D numerical simulations to assess and enhance the efficiency of supersonic missiles. The study focuses on a comparative analysis of aerodynamic performance between conical and ogive nose shapes. Mesh generation was accomplished using Gambit, while the governing flow equations, particularly under high Mach numbers and varying angles of attack for two models, were solved using the commercially available software ANSYS FLUENT 17.1.



## 2. Geometry

Figure 1 illustrates the missile, where  $D$  represents the diameter of the missile, and  $L$  represents the length of the missile. The missile is positioned inside a cylindrical structure, as shown in Figure 2. The diameter of the cylindrical structure, denoted as  $d$ , is five times the diameter of the missile ( $d = 5D$ ). This ratio helps minimize the influence of the cylinder's side surfaces on the flow characteristics around the missile. Additionally, the length of the cylindrical structure, denoted as  $l$ , is four times the length of the missile ( $l = 4L$ ).

After creating five simulation cases with mesh sizes of 2.0, 2.2, 2.3, 2.4, and 2.5 million cells respectively to investigate mesh independence, the results reveal that with 2.0 million cells, convergence is achieved, surpassing the user-defined tolerance threshold. However, upon increasing the grid resolution to 2.2 million cells, convergence is achieved with residuals of  $10^5$  and imbalances of less than 1%. The simulated value falls within the acceptable range compared to the experimental results of Şumnu et al. (2020) in Table 1. Upon further grid refinement to 2.2–2.5 million cells, the simulated value also falls within the acceptable range. This suggests that a solution value independent of grid resolution has been reached. For subsequent analysis, the case with 2.2 million cells can be utilized as it provides results within the user-specified tolerance Figure 3.

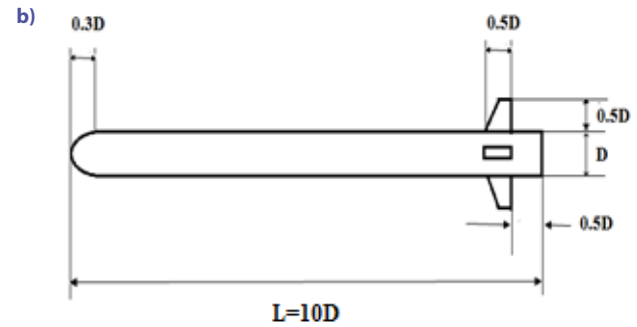


Figure 1. Missiles dimensions

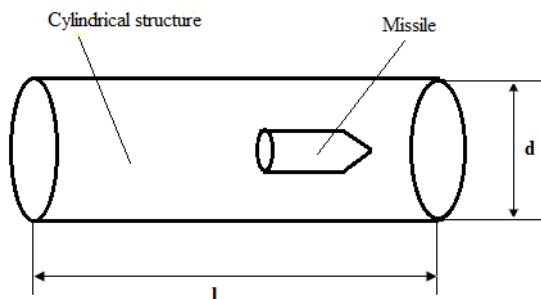


Figure 2. Control volume dimensions

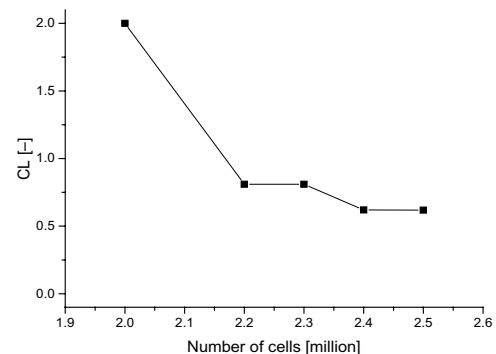


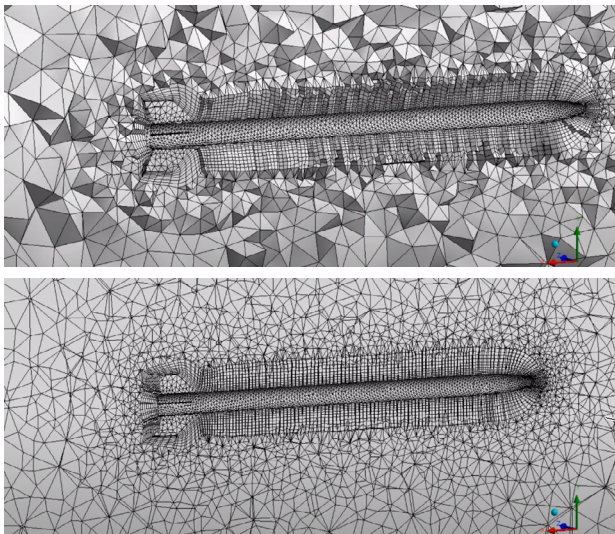
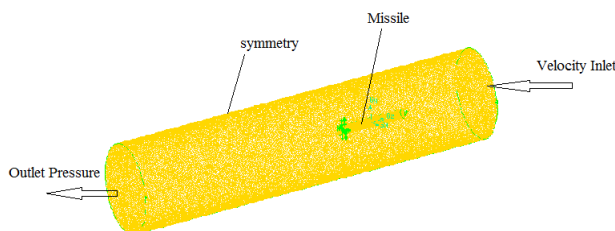
Figure 3. Mesh independence study

**Table 1.** Mesh independence study

Element Number [M]	CL [-]	CL Exp (Şumnu et al., 2020) [-]
2.0	2.0	0.77
2.2	0.81	
2.3	0.81	
2.4	0.62	
2.5	0,6182	

The mesh is made up of a combination of hexahedral and tetrahedral elements (Goucem, 2024). Boundary layer elements are used in the viscous region close to the body, while tetrahedral elements occupy the remaining fluid volume. The smallest boundary layer elements in the mesh measure 0.005 mm. Furthermore, ten layers of boundary layer elements with a growth rate of 1.3 were created on the missile's surface. The entire grid contains roughly 2.2 million elements, as shown in Figure 4.

The 3D simulation occurs within the calculated domain. The inlet boundary condition was specified for various Mach numbers: 1.5, 2, 2.5, 3, 3.5, 4.5, and 5, at angles of attack of 0°, 10°, and 20°. The air density was set to 1.225 kg/m<sup>3</sup>, matching the conditions during wind tunnel testing. At the outlet, the gauge pressure was set to zero. The wall was treated with a symmetry boundary condition due to the different wind orientations Figure 5.

**Figure 4.** The generated mesh structure**Figure 5.** Boundary conditions

### 3. Numerical modeling

The investigation involves examining the fluid dynamics within the defined computational domain, which is assumed to be three-dimensional (3D), unsteady, compressible, and characterized by turbulent behavior. The K- $\omega$  SST turbulence model is utilized for turbulence modeling. The governing equations considered are the unsteady Reynolds-averaged Navier–Stokes (URANS) equations, and their numerical solution is achieved using the finite volume method with a standard pressure-based solver. The pressure-velocity coupling is managed using the SIMPLE scheme. A second-order upwind approach is employed for both momentum and modified turbulent viscosity. To incorporate the time-varying nature of the flow in the computations, the continuity equation for unsteady 3D compressible flow is expressed as follows:

$$\frac{\partial \rho}{\partial t} + \frac{\partial \rho U_i}{\partial x} + \frac{\partial \rho U_j}{\partial y} + \frac{\partial \rho U_k}{\partial z} = 0, \quad (1)$$

where:  $\rho$  – Density of the fluid (kg/m<sup>3</sup>),  $t$  – Time (s),  $U_{(i,j,k)}$  – Velocity vector (m/s).

The Navier-Stokes equations represent a system of second-order nonlinear partial differential equations. Their solution entails establishing three equations corresponding to the three unknowns (velocity components) governing fluid flow. Furthermore, incorporating suitable boundary conditions is essential to enable the resolution of these equations.

$$\frac{\partial U_i}{\partial t} + U_i \frac{\partial U_i}{\partial x_i} = -\frac{1}{\rho} \frac{\partial U_i}{\partial x_i} + \nu \frac{\partial^2 U_i}{\partial x_i^2} + \frac{F_i}{\rho}, \quad (2)$$

where:  $F_i$  – Body forces (N/m<sup>3</sup>).

The Shear-Stress Transport (SST) k- $\omega$  turbulence model is recognized for its versatility and widespread utilization in aerodynamic simulations. This turbulence model, characterized by two equations for eddy viscosity, serves as a hybrid by seamlessly integrating features from both the k- $\omega$  and k-epsilon turbulence models. By strategically combining the inherent strengths of each model, the SST k- $\omega$  model enhances overall performance and applicability.

The k- $\omega$  model demonstrates particular proficiency in simulating flow within the viscous sublayer, where fluid dynamics near solid boundaries are significantly influenced by viscosity effects. In this context, the k- $\omega$  model excels in capturing the complex dynamics of the boundary layer, offering precise predictions of turbulence behavior in close proximity to walls.

Turbulence kinetic energy equation:

$$\frac{\partial}{\partial t} (\rho K) + \frac{\partial U_i}{\partial x_j} (\rho U_i K) - \frac{\partial}{\partial x_j} \left( \left( \mu + \frac{\mu_t}{\sigma_k} \right) \frac{\partial K}{\partial x_j} \right) = \tau_{ij} \frac{\partial U_i}{\partial x_j} - \beta^* K \omega, \quad (3)$$

where:  $\omega$  – Dissipation rate of turbulent kinetic energy (m<sup>2</sup>/s<sup>3</sup>),  $k$  – Turbulent kinetic energy (m<sup>2</sup>/s<sup>2</sup>),  $\mu$  – Viscosity (N.s/m<sup>2</sup>),  $\mu_t$  – Viscosity at the wall (N.s/m<sup>2</sup>).



Specific dissipation rate:

$$\frac{\partial}{\partial t}(\rho\omega) + \frac{\partial U_i}{\partial x_j}(\rho U_j \omega) - \frac{\partial}{\partial x_j} \left( \left( \mu + \frac{\mu_t}{\sigma_\omega} \right) \frac{\partial \omega}{\partial x_j} \right) = \frac{\rho \gamma}{\mu_t} \tau_{ij} \frac{\partial U_i}{\partial x_j} - \beta^* K \omega^2 + 2\rho(1 + F_1)\sigma_\omega \frac{\partial K}{\partial x_j} \frac{\partial \omega}{\partial x_j} \quad (4)$$

where:  $\beta$ ,  $\beta^*$ ,  $a_1$ ,  $\sigma_k$ ,  $\sigma_\omega$  – Interior Region Constants.

Turbulent viscosity

$$\mu_t = \frac{\rho K / \omega}{\max(1, \Omega F_2 / a_1 \omega)} \quad (5)$$

where:  $\Omega$  – Local vorticity.

The function F1 and F2 is defined by

$$F_1 = \tanh \left( \left( \min \left[ \max \left( \frac{2\sqrt{K}}{\beta^* \omega y}, \frac{500\nu}{y^2 \omega}, \frac{4\sigma_\omega 2^K}{CD_{k\omega} y^2} \right) \right] \right)^4 \right); \quad (6)$$

$$F_2 = \tanh \left[ \left( \frac{\sqrt{K}}{\beta^* \omega y}, \frac{500\nu}{y^2 \omega} \right) \right]^2 \quad (7)$$

where:  $\nu$  – Kinematic viscosity ( $m^2/s$ ),  $F_1$ ,  $F_2$  – Functions,  $y$  – Distance to the nearest wall (m),  $\nu$  – Kinematic viscosity ( $m^2/s$ ),  $CD_{k\omega}$  – Cross-diffusion term.

### 3.1. Calculation procedure

The calculation domain is considered three-dimensional (3D), unsteady, compressible, and turbulent, employing the k- $\omega$  SST turbulence model. The governing equations utilized are the unsteady Reynolds-Averaged Navier-Stokes (URANS) equations. These equations are solved using the numerical finite volume method via the standard pressure-based solver.

The computational grid is designed to accurately capture the intricate flow features, ensuring that boundary layers, wake regions, and interaction zones are adequately resolved. The pressure-velocity coupling is managed using the SIMPLE (Semi-Implicit Method for Pressure-Linked Equations) scheme, which is well-suited for handling compressible flows.

Both momentum and modified turbulent viscosity are addressed using the second-order upwind approach to enhance solution accuracy. This method helps to reduce numerical diffusion and provides a more precise representation of the flow field.

Additionally, the boundary conditions are meticulously defined: the inlet boundary condition involves specified Mach numbers, the outlet boundary condition is set to a constant pressure, and the wall boundary condition assumes no-slip conditions. The mesh independence study is conducted to ensure that the results are not affected by the grid size, verifying the reliability of the computational model.

## 4. Results and discussion

In this section, the outcomes of a comparative numerical investigation aimed at evaluating the aerodynamic

performance of supersonic missiles with conical and ogive nose configurations are presented, employing computational fluid dynamics. The analysis includes examinations of both drag coefficients Figures 6, 7, and 8 and lift coefficients Figures 9, 10, and 11 across varying Mach numbers and angles of attack (AoA) of  $0^\circ$ ,  $10^\circ$ , and  $20^\circ$ . Specifically, computations were conducted for missiles equipped with both conical and ogive noses. Insights from prior studies were integrated into a comparative analysis, with the results compared to the experimental data from the study (Şumnu et al., 2020), which constituted a pivotal component of the primary dataset. Additionally, velocity contours for missiles featuring conical and ogive noses at an angle of attack (AoA) of  $0^\circ$  are presented in Figures 12, 13.

### 4.1. Drag coefficients and the impact of angle of attack

The comparative numerical exploration delved into the aerodynamic performance of supersonic missiles, specifically focusing on conical and ogive nose configurations using computational fluid dynamics simulations. Drag coefficient curves were meticulously scrutinized across various Mach numbers and angles of attack ( $0^\circ$ ,  $10^\circ$ , and  $20^\circ$ ), illustrated in Figures 6, 7, and 8.

Notably, the observed trends unveiled insightful behaviors of drag coefficients for both nose configurations. A consistent decrease in drag coefficient was observed with increasing Mach number, regardless of the nose shape. This reduction is attributed to compressibility effects at higher Mach numbers, where shock waves generated around the missile decrease in intensity, thus reducing aerodynamic drag. The analysis revealed that drag coefficients for conical noses surpassed those of ogive noses across various conditions. This difference is due to the distinct flow behavior around the nose geometries, with conical noses generating stronger shock waves and larger pressure gradients, consequently leading to increased aerodynamic drag.

Additionally, the impact of the angle of attack on the drag coefficient is crucial for comprehending the

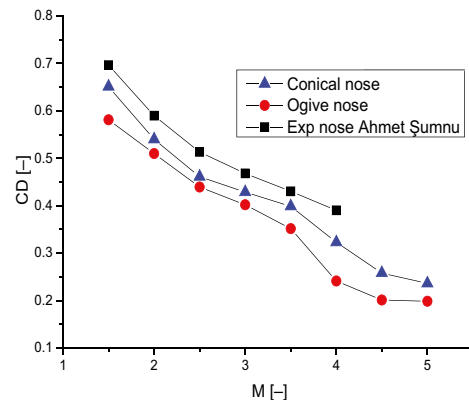
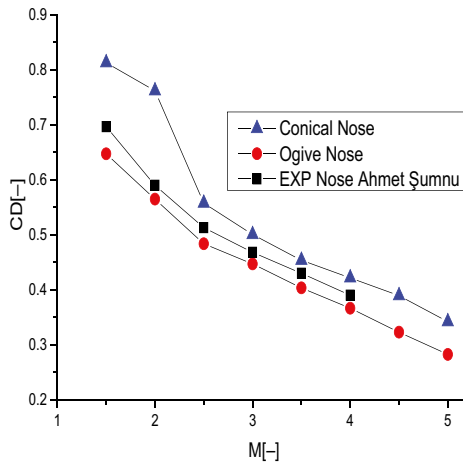
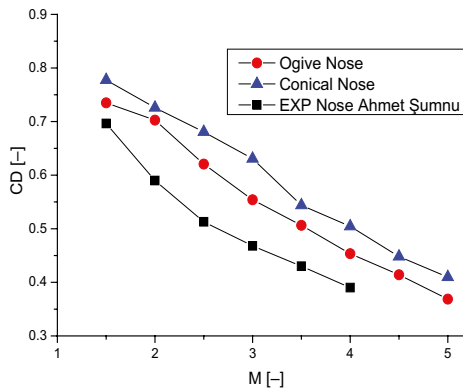


Figure 6. Curves of the drag coefficient changing with the Mach numbers for angle of attack  $0^\circ$



**Figure 7.** Curves of the drag coefficient changing with the Mach numbers for angle of attack 10°



**Figure 8.** Curves of the drag coefficient changing with the Mach numbers for angle of attack 20°

aerodynamic performance of missiles equipped with conical and ogive heads. As the angle of attack rises from 0° to 20°, the drag coefficients of these missiles display distinct trends, diverging based on the head design. An increase in angle of attack results in higher drag coefficients for both configurations, primarily due to the increased frontal area exposed to airflow, leading to higher pressure drag as flow separates from the missile's surface. However, the rate of increase in drag coefficient varies significantly between the two configurations. Conical noses generally exhibit a higher rate of increase in drag coefficient compared to ogive noses. This variation highlights the influence of the angle of attack on the aerodynamic characteristics of supersonic missiles.

Moreover, the results indicate that the aerodynamic performance of supersonic missiles is significantly influenced by both the nose shape and the angle of attack. The conical nose configuration, while more susceptible to increased drag at higher angles of attack, provides valuable insights into the behavior of supersonic flow around sharp geometries. Conversely, the ogive nose configuration, with

its smoother flow characteristics, offers a distinct advantage in reducing aerodynamic drag, particularly at lower angles of attack.

## 4.2. Lift coefficients and the impact of angle of attack

The analysis of lift coefficient curves as a function of Mach number for various angles of attack (0°, 10°, and 20°) in supersonic missiles equipped with conical and ogive noses revealed intriguing behaviors. Illustrated in Figures 9, 10, and 11, the lift coefficients exhibited similar trends to the experimental lift coefficient referenced in Şumnu et al. (2020).

The observed trends demonstrated a decrease in lift coefficient with increasing Mach number for both conical and ogive nose configurations. This reduction is primarily due to compressibility effects at higher Mach numbers, where airflow around the missile becomes more compressible, resulting in reduced lift generation. The analysis also underscored that the lift coefficient for conical nose shapes exceeded that of ogive shapes under the examined conditions. This discrepancy is attributed to the distinct flow dynamics surrounding conical noses, which tend to generate stronger lift forces compared to the smoother flow patterns observed around ogive noses. Specifically, there was a 2–11% increase in the lift coefficient for conical heads relative to ogive heads.

Furthermore, the influence of the angle of attack on the lift coefficient reveals a consistent trend across both conical and ogive nose shapes. As the angle of attack increases from 0° to 20°, the lift coefficient for both configurations decreases. This decline can be attributed to heightened flow separation and diminished airfoil effectiveness at higher angles of attack. With increased deviation from the nominal angle of attack, the airflow over the missile's surface becomes more disrupted, resulting in reduced lift generation. This observation underscores the critical role of angle of attack in governing the aerodynamic behavior of supersonic missiles, highlighting the challenges associated with maintaining lift performance under varying flight conditions.

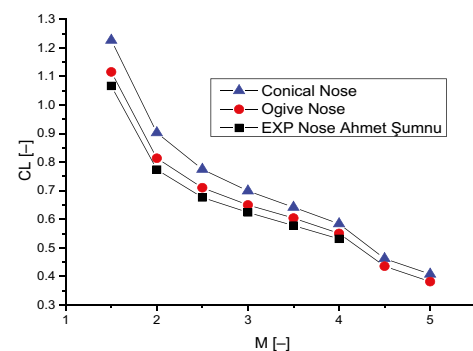


**Figure 9.** Curves of the lift coefficient changing with the Mach numbers for angle of attack 0°

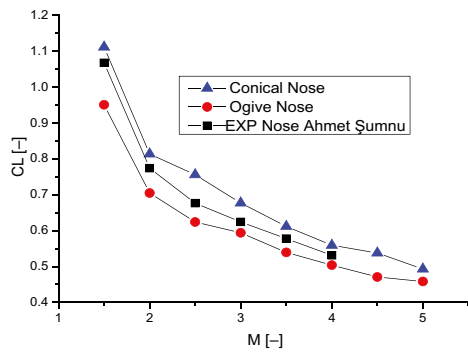


**Figure 10.** Curves of the lift coefficient changing with the Mach numbers for angle of attack  $10^\circ$

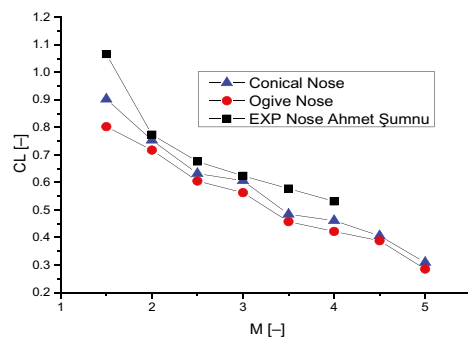


**Figure 11.** Curves of the lift coefficient changing with the Mach numbers for angle of attack  $20^\circ$

Moreover, the impact of angle of attack on the aerodynamic performance of missiles is crucial for understanding their operational limits and effectiveness. At lower angles of attack, both conical and ogive noses perform relatively well, maintaining higher lift coefficients. However, as the angle of attack increases, the aerodynamic performance diverges, with conical noses exhibiting a more pronounced reduction in lift compared to ogive noses. This behavior is particularly important for missile design and optimization, as it affects maneuverability and stability during flight.

In summary, the combined analysis of drag and lift coefficients, along with the impact of angle of attack, provides a comprehensive understanding of the aerodynamic performance of supersonic missiles. The distinct behaviors of conical and ogive nose configurations under varying conditions highlight the importance of selecting the appropriate nose design based on specific mission requirements and flight profiles. The insights gained from this study can inform future missile design, contributing to enhanced aerodynamic efficiency and overall performance.

### 4.3. Velocity contours

The analysis of velocity contours in the present study reveals intriguing disparities between missiles equipped with conical and ogive noses (Figures 12, 13). Notably, the examination of shock waves indicates a substantial

discrepancy in their characteristics, particularly in terms of angle and intensity. It is observed that the shock wave in missiles featuring a conical nose occurs at a smaller angle compared to those with an ogive nose. This variation suggests inherent differences in the flow behavior around the two nose configurations. Furthermore, a striking finding emerges from the analysis of velocity magnitudes, particularly evident in the significant change observed between missiles with ogive and conical noses.

In Figure 12, the velocity contours for the ogive nose exhibit a streamlined flow pattern with gradual acceleration around the nose and along the missile body. The ogive nose promotes a more laminar flow, resulting in weaker shock waves and smaller pressure gradients. This smoother flow pattern minimizes aerodynamic drag, contributing to more efficient flight characteristics. The gradual transition of velocity colors from blue to red indicates a consistent increase in velocity with minimal disruption, highlighting the ogive nose's ability to maintain flow attachment and reduce drag. Specifically, the velocity contour data illustrate a remarkable difference in velocity magnitude, with missiles sporting a conical nose exhibiting velocities as high as 1600 m/s, while those with an ogive nose reach only 770 m/s.

Conversely, in Figure 13, the velocity contours for the conical nose show a more abrupt change in flow velocity near the nose, with stronger shock waves and higher pressure gradients. The conical nose's sharper geometry

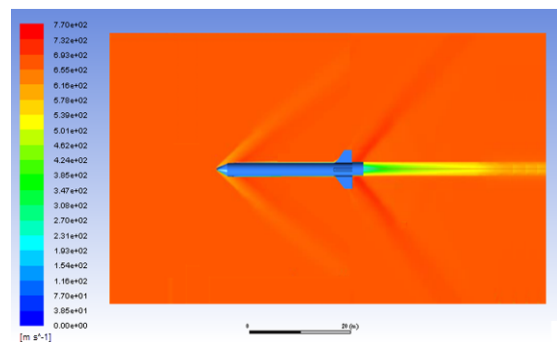


**Figure 12.** Velocity contours for a missile with an ogive nose at an angle of attack of  $0^\circ$

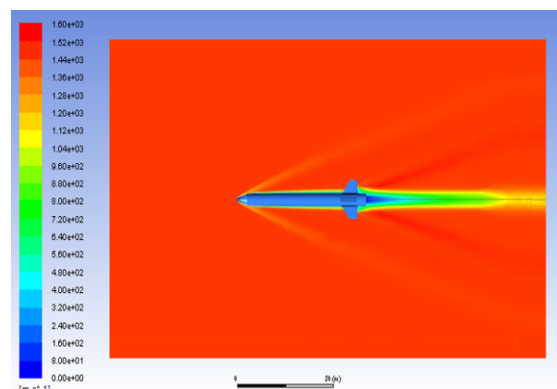


**Figure 13.** Velocity contours for a missile with a conical nose at an angle of attack of  $0^\circ$

causes significant disturbance in the flow, leading to higher aerodynamic drag. The contours reveal a pronounced acceleration of flow at the nose tip, indicated by the rapid transition from blue to red, followed by a turbulent wake region. This increased turbulence and flow separation around the conical nose contribute to the observed higher drag coefficients.

The differences in flow behavior between the ogive and conical noses are further emphasized by the extent of flow separation. The conical nose induces a more substantial flow separation, creating a larger low-pressure wake region behind the missile, which is a primary factor in increased aerodynamic drag. In contrast, the ogive nose maintains better flow attachment, resulting in a smaller wake and lower drag. These visualizations and analyses underscore the critical impact of nose geometry on the aerodynamic performance of supersonic missiles. The ogive nose, with its smoother flow and reduced drag, is advantageous for achieving higher speeds and better fuel efficiency. However, the conical nose, despite its higher drag, may offer benefits in terms of lift generation and stability at certain flight conditions. Understanding these trade-offs is essential for optimizing missile design to balance between aerodynamic efficiency, stability, and performance requirements.

The reason for the significant difference in velocities between missiles with conical and ogive noses can be attributed to the aerodynamic characteristics and flow dynamics associated with each nose configuration. Several factors contribute to this variation in velocities:

**Nose Geometry:** Conical and ogive noses have distinct shapes that result in different aerodynamic behaviors. Conical noses typically produce stronger shock waves and larger pressure gradients compared to ogive noses due to their sharper leading edges. This can lead to more efficient acceleration and higher velocities for the airflow around missiles with conical noses.

**Shock Wave Formation:** The shock wave formed around the nose of a missile plays a crucial role in dictating the airflow behavior and resultant velocities. The angle and intensity of the shock wave differ between conical and ogive noses, affecting how the airflow interacts with the missile and its surroundings. The smaller angle of the shock wave for missiles with a conical nose could contribute to more efficient airflow acceleration and higher velocities compared to missiles with an ogive nose.

**Flow Separation:** Differences in nose geometry can also influence flow separation patterns, where the airflow detaches from the missile's surface. Conical noses may experience less flow separation compared to ogive noses, leading to smoother airflow and potentially higher velocities.

**Boundary Layer Effects:** The boundary layer, a thin layer of air adjacent to the missile's surface, plays a significant role in aerodynamic performance. Variations in nose geometry can affect boundary layer behavior, influencing drag and velocity characteristics. Conical noses may experience reduced boundary layer separation and drag, allowing for higher velocities compared to ogive noses.

## 5. Conclusions

The comparative numerical investigation into the aerodynamic performance of supersonic missiles with conical and ogive nose configurations, conducted through computational fluid dynamics simulations across varying Mach numbers between 1 and 5 and angles of attack (AoA) of 0°, 10°, and 20°, has yielded significant insights into their aerodynamic behaviors.

### ■ Main Contributions and Novelty

This research provides a comprehensive analysis of the drag and lift coefficients for both conical and ogive nose configurations under different flight conditions. The main contribution lies in the detailed comparison of these configurations, highlighting the distinct aerodynamic characteristics that arise from their geometrical differences. The novelty of this study is in its meticulous examination of how these nose shapes influence the aerodynamic performance of supersonic missiles, particularly in terms of drag and lift under varying angles of attack and Mach numbers.

### ■ Key Findings

**Drag Coefficients:** The study reveals that the drag coefficient for conical noses consistently exceeds that of ogive noses across various conditions. This difference is attributed to the stronger shock waves and larger pressure gradients generated by the conical noses. Specifically, a notable 14% increase in the drag coefficient is observed for conical heads compared to ogive heads at higher angles of attack.

**Lift Coefficients:** The lift coefficient analysis indicates a decrease with increasing Mach number for both configurations due to compressibility effects. However, conical noses exhibit a higher lift coefficient compared to ogive noses, with a 2–11% increase in the lift coefficient for conical heads relative to ogive heads.

**Impact of Angle of Attack:** The angle of attack significantly influences the aerodynamic performance, with both drag and lift coefficients increasing with higher angles of attack. The conical noses show a higher rate of increase in drag coefficient compared to ogive noses, while both configurations experience a decrease in lift coefficient as the angle of attack increases from 0° to 20°.

### ■ Practical Applications

The findings from this study have practical implications for the design and optimization of supersonic missiles. The insights into the drag and lift characteristics of different nose shapes can inform decisions on nose geometry to balance aerodynamic efficiency, stability, and performance requirements. The conical nose, while generating higher drag, may offer benefits in terms of lift and stability at certain flight conditions, making it suitable for specific mission profiles.

### ■ Future Work

Future research should focus on further refining the computational models to include more complex flow conditions and additional geometrical variations. Experimental validation of the simulation results under a broader range of flight conditions would also enhance the robustness of the findings. Additionally, exploring the effects of different



materials and surface treatments on the aerodynamic performance could provide valuable information for optimizing missile design.

In summary, this research underscores the intricate relationship between nose configuration, angle of attack, and aerodynamic performance in supersonic missiles, offering valuable insights for the aerospace engineering community and contributing to the advancement of missile design technology.

## Author contributions

M. Goucem created the Gambit mesh for the missile and conducted computational fluid dynamics (CFD) simulations using ANSYS Fluent 17.1, as well as developed the mathematical modeling.

The manuscript was written with the contribution of all authors. All authors participated in result discussions, reviewed, and approved the final version of the manuscript.

## References

- Almawla, A., Lateef, A., & Kamel, A. (2022). Water flow simulation with computational fluid dynamics (CFD): A review study. *International Review of Civil Engineering (IRECE)*, 13(1), 40–52. <https://doi.org/10.15866/irece.v13i1.20958>
- Bin-Dahalan, N., Suni, A., Shah-Ishak, I., Nik Mohd, A. R., & Mat, S. (2017). Aerodynamic study of air flow over a curved fin rocket. *Journal of Advanced Research in Fluid Mechanics and Thermal Science*, 40(1), 46–58.
- Chen, Y.-C., Gao, X.-B., & Gao, M. (2017). Numerical simulation on rolling characteristics of canard-controlled rockets with a free-spinning tail. *International Journal of Modeling Simulation and Scientific Computing*, 8(2). <https://doi.org/10.1142/S1793962317500611>
- Divakaran, R., Bareto, N., & Srinivas, G. (2020). Aerodynamic performance enhancement of missile using numerical techniques. *Journal of Physics Conference Series*, 1706, Article 012222. <https://doi.org/10.1088/1742-6596/1706/1/012222>
- Doig, G. (2014). Transonic and supersonic ground effect aerodynamics. *Progress in Aerospace Sciences*, 69, 1–28. <https://doi.org/10.1016/j.paerosci.2014.02.002>
- Ghoreyshi, M., Jirasek, A., & Aref, P. S., & Seidel, J. (2022). Computational aerodynamic investigation of long strake-tail missile configurations. *Aerospace Science and Technology*, 127, Article 107704. <https://doi.org/10.2514/6.2022-1535>
- Goucem, M. (2024). Influence of the ambient temperature on the efficiency of gas turbines. *Fluid Dynamics and Materials Processing*, 20(10), 2265–2279. <https://doi.org/10.32604/fdmp.2024.052365>
- Goucem, M., & Khiri, R. (2023). Optimizing supersonic rocket efficiency: A numerical analysis of aerodynamic characteristics and angle of canard deflection. *International Review of Aerospace Engineering (IREASE)*, 16(5), 207–214. <https://doi.org/10.15866/irease.v16i5.24129>
- Julian, J., Iskandar, W., Wahyuni, F., Adhynugraha, M. I., & Hasim, F. (2023). Numerical study on aerodynamics characteristics of R-HAN122 along with nose modification. *International Review of Aerospace Engineering (IREASE)*, 16(3), 123–132. <https://doi.org/10.15866/irease.v16i3.23400>
- Karpenko, M., & Bogdevičius, M. (2020). Investigation of hydrodynamic processes in the system – “pipeline-fittings”. In K. Gopalakrishnan, O. Prentkovskis, I. Jackiva, & R. Junevičius, *TRANSBALTICA XI: Transportation Science and Technology. TRANSBALTICA 2019. Lecture Notes in Intelligent Transportation and Infrastructure* (pp. 331–340). Springer. [https://doi.org/10.1007/978-3-030-38666-5\\_35](https://doi.org/10.1007/978-3-030-38666-5_35)
- Karpenko, M., Stosiak, M., Šukevičius, Š., Skačkauskas, P., Urbanowicz, K., & Deptuła, A. (2023). Hydrodynamic processes in angular fitting connections of a transport machine’s hydraulic drive. *Machines*, 11(3), Article 355. <https://doi.org/10.3390/machines11030355>
- Khanolkar, N. P., Bhushan, B., Siddharth, M., Borrison, E., & Sinha, J. (2018). Analysis of aerodynamic characteristics of a missile configuration. In *2017 International Conference on Infocom Technologies and Unmanned Systems (Trends and Future Directions) (ICTUS)*. IEEE. <https://doi.org/10.1109/ICTUS.2017.8286129>
- Li, Y., Yi, L., Ao, Y., Ma, L., & Wang, Y. (2020). Simulation analysis the aerodynamic characteristics of variable sweep wing missile. *Journal of Physics Conference Series*, 1570(1), Article 012073. <https://doi.org/10.1088/1742-6596/1570/1/012073>
- Marciniak, B. A., Cieśliński, D., & Matyszewski, J. (2023). Verifying the ILR-33 AMBER rocket recovery system by means of a drop test campaign. *International Review of Aerospace Engineering (IREASE)*, 16(1), 9–19. <https://doi.org/10.15866/irease.v16i1.22619>
- Ruchała, P., Placek, R., Stryczniewicz, W., Matyszewski, J., Cieśliński, D., & Bartkowiak, B. (2019). Wind Tunnel tests of influence of boosters and fins on aerodynamic characteristics of the experimental rocket platform. *Transactions on Aerospace Research*, 4(249), 82–102. <https://doi.org/10.2478/tar-2017-0030>
- Sahbon, N., Murpani, S., Michałow, Miedziński, D., & Sochacki, M. (2022). A CFD study of the aerodynamic characteristics of Twardowsky and FOK rockets. *Transactions on Aerospace Research*, 266(1), 35–58. <https://doi.org/10.2478/tar-2022-0003>
- Şumnu, A., & Guzelbey, İ. H. (2023). The effects of different wing configurations on missile aerodynamics. *Journal of Thermal Engineering*, 9(5), 1260–1271. <https://doi.org/10.18186/thermal.1377200>
- Şumnu, A., Guzelbey, İ. H., & Öğücü, O. (2020). Aerodynamic shape optimization of a missile using a multiobjective genetic algorithm. *International Journal of Aerospace Engineering*, 2020, 1–17. <https://doi.org/10.1155/2020/1528435>
- Yi, L., Li, Y., Ma, L., Ao, Y., & Wang, Y. (2021). Analysis of aerodynamic characteristics of missile with different sweep angle under supersonic condition. *Journal of Physics: Conference Series*, 1802(4), 1–5. <https://doi.org/10.1088/1742-6596/1802/4/042003>